Analog Experiments of Icy Moon Subsurface Ocean Dynamics. E. K. Hawkins[1], F. Lynch[2,3], and J. E. Simkin[2]. [1]Loyola Marymount University, Department of Physics (Emily.Hawkins@lmu.edu), [2]Loyola Marymount University, Department of Mechanical Engineering, [3]University of Michigan Ann Arbor, Department of Mechanical Engineering.

Introduction: Icy moons with subsurface oceans, such as Europa and Enceladus, may possess environments that are suitable for harboring life [1-3]. In addition to the presence of stable liquid water, an astrophysical body cannot be classified as being habitable without the existence of essential chemical ingredients including carbon, hydrogen, oxygen, etc. [4]. A likely source of these elements is the seafloor, where hydrothermal vents are thought to exist [5, 6]. Detailing the dynamics of rotating convective turbulence in the subsurface oceans of icy satellites is crucial in order to constrain the potential transport of vital nutrients from the seafloor to the ice-ocean interface [7, 8].

Several critical outstanding questions exist surrounding the details of particle transport and availability within the bulk ocean and ice-ocean interface of icy satellites including: the exact mechanism(s) by which transport might occur, the existence (or lack thereof) of a stable layer with light solutes at the base of the ice shell, the influence of local versus global circulation on entrained particles, and more [9-11]. Towards this end, a new experimental apparatus specifically designed for studies of icy satellite subsurface ocean and ice-ocean interface dynamics has been created and will be used to answer these outstanding questions. The details of this novel device and its capabilities, as well as plans for initial experimentation will be presented.

Methodology: As shown in Figure 1, the experimental chamber consists of an acrylic cylindrical sidewall bounded by two smooth, rigid aluminum blocks that sit atop a custom-designed rotating table. Containers of varied heights ranging between 10 to 60 cm (all 40 cm diameter) can be filled with saltwater (NaCl or $MgSO_4$) of differing salinities (0 to 350 g/L). The cylindrical convection chamber is representative of a parcel of bulk oceanic fluid at polar regions where the direction of convection is aligned with that of rotation. Recent studies show that polar measurements of rotating convective dynamics are representative of the dynamics of the entire spherical shell layers of astrophysical bodies far past convective onset [12].

Thermal Capabilities. Convection is driven via a heating pad placed below the bottom block while cool water is simultaneously passed through the top block. The apparatus is capable of rotating at speeds between 0 to 80 rotations per minute, and heating power can range from 0 to 5,000 Watts (corresponding to temperature gradients between 0.5 to 90°C). Small, high precision temperature sensors can be placed at the fluid boundaries and can be inserted directly into the fluid layer through the top block to characterize fluid heat transfer, both globally and locally.

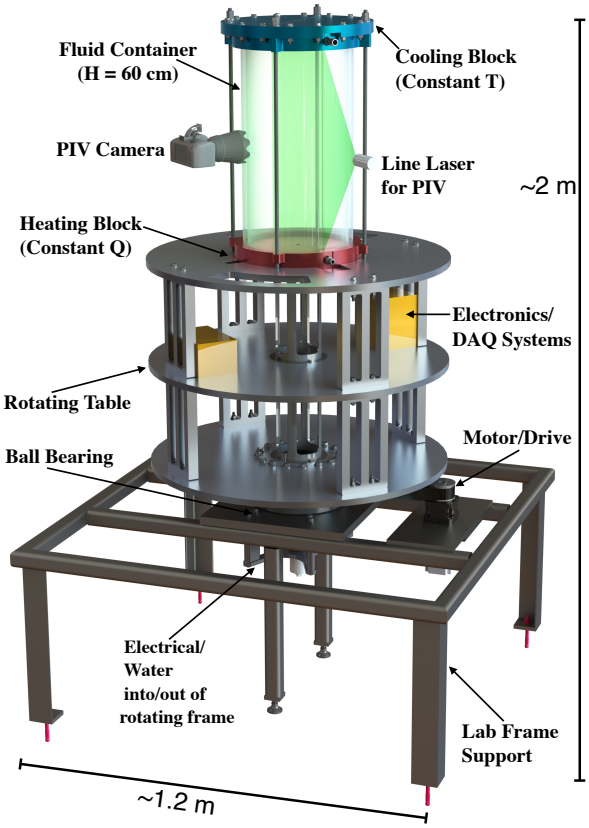

Figure 1: Schematic of the novel icy satellite convection device at Loyola Marymount University (LMU). The apparatus consists of a convection chamber atop a rotating turntable with temperature, velocity, and length scale measurement capabilities.

Particle Image Velocimetry. The fluid is seeded with neutrally buoyant reflective particles (20 μm hollow glass spheres), and a Canon Rebel T8i camera is used with a 2.3 Watt continuous green line laser to carry out particle image velocimetry (PIV) measurements [13, 14]. Two-dimensional velocity fields obtained using PIV are used to characterize vertical convective velocities and characteristic flow length scales. Simultaneous measurements of heat transfer, velocities, and length scales are necessary due to their coupled nature and will allow for detailed characterization

of the convective dynamics relevant to bulk subsurface oceans [15, 16].

Topography and Particle Entrainment. Polylactic acid (PLA) or polyethylene terephthalate glycol (PETG) 3D printed topography of an analog seafloor with different shapes and sizes (including that of Earth's) can be used to study the effect of seafloor topography on particle entrainment. Analog spherical and non-spherical entrainment particles can be made of silicon carbide, mono- and poly-disperse polystyrene, polyvinyl chloride, and/or polymethyl methacrylate (all of size ≤ 5 μm) [17-19].

Ice Formation Technique. Temperature gradients can be adjusted such that the top layer of convecting fluid will freeze to varying degrees, simulating the ice-ocean interface at the top of the experimental chamber. To do this, a 50-50 mixture of ethylene glycol-water (EG-W) can be passed through the top thermal block of the convection chamber using a custom low-temperature industrial recirculating chiller. This EG-W mixture has a low freezing point (-36°C) and can thus cool the top of the saltwater layer within the convection chamber to its freezing temperature (~-2°C).

Dynamical Regime Exploration. The full range of experimental parameters described will be investigated and systematically varied to explore different regimes of rotating saltwater convection [20-22]. Figure 2 shows the predicted heat transfer behavioral regimes of rotating convection. The y-axis shows the Rayleigh number, Ra, which represents the strength of thermal forcing while the x-axis shows the Ekman number, E, which represents the rotational strength on the fluid. The capabilities of the LMU device are highlighted by the green box and overlap with numerical models (stars) while expanding the parameter space region that can be covered by analog models (i.e. achieving rotating convective turbulence). Predictions for Titan (T, grey), Ganymede (G, blue), Europa (Eur, teal), and Enceladus (Enc, pink) lie in the upper right corner, indicating that rotation and thermal forcing strongly influence oceanic convection.

The predictions for differing convective regimes are labeled and bounded by solid or dashed lines in Fig. 2. Importantly, the green parameter space covered by the new LMU experiment includes all of the predicted regimes, from subcritical to non-rotating style heat transfer. Thus, the LMU device is capable of exploring all of the predicted heat transfer regimes of rotating convection and transitions therein. Coupled to the heat transfer behavior shown in Fig. 2 is momentum transfer. Recent studies show that velocity behavior in rotating convection systems is robustly governed by a diffusion-free balance between the rotation, inertia, and buoyancy in the system [15, 16, 23]. Experimental work herein will further confirm the connection between heat and momentum transfer and the tie to particle entrainment for icy satellite subsurface oceans.

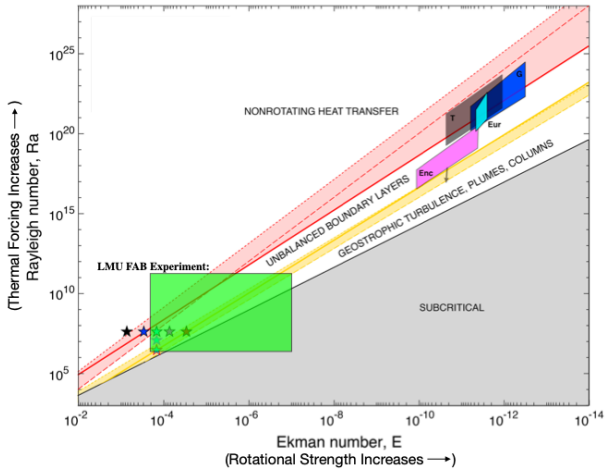

Figure 2: Predicted heat transfer behavioral regimes of bulk fluid convection, where the Rayleigh number representing the strength of thermal forcing is plotted versus the Ekman number, which represents rotational strength. See text for more details. Adapted from [8].

References: [1] Vance S. D. et al. (2018) *JGR, 123.1,* 180-205. [2] Hendrix A. R. et al. (2019) *Astrobio, 19.1,* 1-27. [3] Howell S. M. and Pappalardo R. T. (2020) *Nat Comm, 11.1* 1-4. [4] Grasset O. et al. (2013) *P & SS, 78,* 1-21. [5] Russell M. J. et al. (2014) *Astrobio, 14.4* 308-343. [6] Hsu H. W. et al. (2015) *Nature, 519* 207-210. [7] Schoenfeld A. M. et al. (2023) *Nat Rev E & E,* Accepted. [8] Soderlund K. M. (2019) *GRL, 46.15.* [9] Soderlund K. M. et al. (2020) *Space Sci Rev, 216.5* 1-57. [10] Carnahan E. et al. (2021) *EPSL, 563.* [11] Melwani Daswani M. et al. (2021) *GRL 48.18.* [12] Gastine T. and Aurnou J. M. (2023) *JFM, 954.* [13] Meunier P. and Leweke T. (2003) *Fluids, 35.5* 408-421. [14] Lemasquerier D. et al. (2020) *Nat Phys, 16.6* 695-700. [15] Hawkins E. K. et al. (2023) *Fluids,* In Review. [16] Schwaiger, T. et al. (2021), *GJI, 224.3,* 1890-1904. [17] Lavorel, G. and Le Bars M. (2009) *PRE, 80.4.* [18] Herbert E. et al. (2018) *JFM, 843* 778-809. [19] Homan T. et al. (2020) *PRE, 5.10.* [20] Lobo A. H. et al. (2021) *Nat Geo, 14.4* 185-189. [21] Zeng Y. and Jansen M. F. (2021) *PSJ, 2.4* 151. [22] Bire S. et al. (2021) *JGR, 127.* [23] Aurnou J. M. et al. (2020) *PRR, 2.4.*